THE POTENTIAL APPLICATION OF FLOW CONTROL TO HELICOPTER ROTOR BLADES

O C Kenning
I W Kaynes
J V Miller

QinetiQ

Farnborough, Hampshire, UK

Abstract

A range of flow control devices are reviewed for their suitability to suppress or eliminate various aerodynamic flow phenomena. Specifically, those devices which may lend themselves to control the flow on helicopter rotor blades are identified. Four types of flow control device are identified as possible candidates, namely (i) air-jet vortex generators, (ii) sub-boundary layer vortex generators, (iii) surface blowing circulation control and (iv) movable flaps.

As an extension to this work, Computational Fluid Dynamics (CFD) calculations are performed on a static RAE9645 aerofoil at 18° incidence incorporating co-rotating air-jet vortex generators at 12% chord. The results are compared to relevant experimental data. It was found that the Spalart-Allmaras turbulence model showed promise in being able to recreate the beneficial effects of air-jet vortex generators to delay flow separation at high incidence. With this model the normal lift coefficient was increased from 1.22 to 1.65, corresponding well with experiment.

In addition, a rotor performance code was used to predict the operational advantages of employing air-jet vortex generators on helicopter rotor blades. This study indicated increases in forward speed of around 20kts were possible, but the possibility of increasing the all-up mass indicated less benefit.

Nomenclature

AJVG	air-jet vortex generator
c	aerofoil chord
C_f	skin friction coefficient
C_N	normal force coefficient
C_p	pressure coefficient
C_μ	(or Cmu) blowing momentum coefficient, $(m_j.V_j)/(\frac{1}{2}\rho_\infty U_\infty^2 c)$
CC	circulation control
m_j	single air-jet mass flow rate
M_∞	freestream Mach number
Re_c	Reynolds number based on aerofoil chord
SBVG	sub-boundary layer vortex generator
s	spanwise distance between AJVGs
u_τ	friction velocity, $(\tau_w/\rho)^{1/2}$
U_∞	freestream velocity
VG	vortex generator
VR	air-jet velocity ratio, V_j/U_∞
V_j	air-jet resultant exit velocity
x	axial length coordinate
y	distance normal to wall
y^+	wall unit, $\rho u_\tau y/\mu$
z	spanwise coordinate
α	angle of attack
ϕ	AJVG pitch angle relative to surface tangent
μ	absolute viscosity
ρ	fluid density
ρ_∞	freestream density
τ_w	wall shear stress
ψ	AJVG skew angle relative to freestream flow

Background

The means to enhance helicopter rotor performance by using passive rotor designs are becoming increasingly limited. Continued rotor design using conventional design approaches are likely to yield ever decreasing performance benefits. The introduction of flow control devices have the potential to provide significant performance gains over current conventional rotor designs. An assessment of various aerodynamic flow control devices have shown that some methods provide the potential for step changes in rotor performance. Compared to traditional passive rotor design, there is the additional advantage that active flow control devices can be scheduled for maximum effect according to mission or flight phase conditions.

The first half of the paper identifies and reviews a wide variety of flow control devices. Each form of flow control is reviewed regarding its suitability for the rotorcraft application, and those devices which are deemed worthy of further investigation are identified.

The second half of the paper discusses the success, or otherwise, of a CFD numerical method employing a wide range of turbulence models in predicting the experimentally observed performance benefits of employing air-jets on a static RAE9645 aerofoil section. Overall performance predictions are also made of a helicopter employing rotor blade air-jet vortex generator technology.

Rotor Design and Flow Control

Historically, flow control research has been directed at enhancing the performance or improving the control of fixed wing aircraft. The application of flow control technology to improve the performance of rotorcraft is very challenging due to the highly unsteady flowfield and wide ranging flow conditions that the rotor experiences. Whilst earlier flow control applications have tended to 'fix' flow problems discovered during aircraft flight test, for example, vortex generators added to an aircraft to control stall behaviour, recent developments have been directed towards core aerodynamic improvements embodied from the design stage.

In terms of rotorcraft performance, the weight-speed envelope is limited by (i) the advancing blade Mach number restricting speed, and (ii) the retreating blade stall restricting weight, as shown in Figure 1. To minimise these restrictions, the basic design requirements for the main section of the rotor blade are as follows: for the advancing blade, minimisation of drag and control of pitching moment, and for the retreating blade, maximum lift without stall or pitching moment break. Suitable rotorcraft flow control devices would require their operation to have a direct positive impact on these design requirements.

Flow Control Device Review

A range of flow control devices have been identified and are detailed in the list below.

1. Vortex generators (VGs) and Sub-boundary layer vortex generators (SBVGs)
2. Gurney flaps
3. Movable flaps
4. Air-jet vortex generators (AJVGs)
5. Surface blowing circulation control (CC)
6. Synthetic/massless jets
7. Surface suction
8. Passive porous or slotted surfaces
9. Bumps or localised shaping
10. Shark skin or riblets

Along with the following text in this section, Table 1 identifies the aerodynamic flow phenomena for which they are suited to control, and also those particular devices which have been identified as suitable for the rotorcraft application.

Each device in terms of its operation and benefit is described in the following sections, along with the perceived effectiveness for the rotorcraft application.

1. Vortex Generators and Sub-Boundary Layer Vortex Generators VGs are an established means to control separation. This is achieved by enhancing mixing between the main air stream and the lower energy flow within the boundary layer, thereby improving the ability of the boundary layer to resist separation. The potential disadvantage of VGs is the parasitic drag of the devices in off-design conditions, likely to be a particular limitation in the wide ranging conditions encountered on a rotor blade.

SBVGs potentially avoid this problem. SBVGs are low profile devices which remain within the low energy flow in the boundary layer and can thus be expected to have low drag. Ashill, Fulker and Hackett, Ref. 1, investigated the effect of SBVGs in the DERA Boundary Layer Tunnel for flows with zero pressure gradient, flows with adverse pressure gradients and for flows over a bump on the roof of the test section. A variety of SBVG geometric configurations were tested. In the zero pressure gradient flow, a two-spaced counter-rotating vane was found to have a much lower streamwise decay of vortex strength than the other tested geometries, including a joined counter-rotating vane. There was an indication that the adverse pressure gradient reduced the effective height of the devices tested in that regime. All the devices reduced the length of separation in the flow over the bump, with spaced counter-rotating vanes being the most effective. In addition to the boundary layer tunnel tests, Ref. 1 describes tests for controlling shock-boundary layer interaction on a 2d aerofoil using two alternative types of SBVG. Counter-rotating vanes and forward wedges were placed at 46.5% chord, approximately 70 device heights upstream of the anticipated shock position. In tests at Mach 0.71, both types of SBVG improved aerofoil performance by delaying trailing edge separation. The counter-rotating vanes gave a 20% increase in maximum normal force (10% increase for the wedges), accompanied by a reduction in drag. At the lower lift coefficient of 0.4, corresponding to the maximum lift/drag ratio, the wedges produced a 5% improvement in lift/drag.

The potential applications of VGs and SBVGs include control of leading edge separation, shock induced separation, and smooth surface separation. Compared to VGs, the SBVGs have the advantage of lower parasitic drag, but in the case of shock induced separation and smooth surface separation, they must be placed closer to the separation line. This may be a significant limitation in the essentially unsteady application of rotorcraft. Another limit may be the varying effect of fixed devices for the oncoming flow at different relative sweep angles to the blade. This may only be alleviated by the significant complication of making the devices retractable.

2. Gurney Flaps A Gurney flap is a small step normal to an aerofoil surface and less than 1% chord height which is mounted at the trailing edge. A flap on the lower surface trailing edge generates an increment of additional lift with a relatively small drag penalty, as measured, for example, at ARA on the RAE9645 aerofoil, Ref. 2. The aerodynamic effect is that the flap modifies the Kutta condition at the trailing edge, similar to an increase of camber, but with a penalty due to increased drag from the thicker trailing edge.

When a Gurney flap is used passively it may be possible to design the local aerofoil section geometry such that the device has no effect for some flow conditions, but provides lift increment under other conditions. The design of such a passive device is a further stage in the difficult compromise process of designing aerofoils for the wide operating conditions of a helicopter rotor blade. The situation is similar for the inclusion of a divergent trailing edge. There may be potential for either device to be actuated, so as to extend only when required, and thus reduce the design compromise problems by eliminating the disturbance when the device is not required. However, Ref. 3 found that although the devices have the attraction of low hinge moments, actuation proves to be more difficult without either the inclusion of mechanical links within the airflow, or a thicker trailing edge which would itself degrade aerofoil performance.

3. Movable Flaps Bechert et al, Ref. 4, described some flow control features found in nature and their application to aircraft. The movable or self-acting flap resulted from the observation that, when a bird is landing, feathers near the rear of the wing pop up. The feathers act to limit the forward spread of the trailing edge separation. Bechert demonstrated the application of the principle on a glider with a flap mounted above the trailing edge. The flap was free to

rotate up from the surface when the conditions were appropriate.

Such a design is unlikely to be acceptable or practical in the conditions of a helicopter rotor blade, with the centrifugal effects tending to make it more difficult to hinge a surface sufficiently freely to operate under small forces. The violent motion of the blade in pitch could also produce unintentional deployment of the flap, with very undesirable consequences for blade efficiency or structural integrity. Commanded operation of a flap could be effective in delaying stall. The possibilities would be to either schedule operation with flight condition and azimuth, deflecting the flap for just the required part of the disc reaching incipient stall, or operating automatically from local pressure sensors on the blade.

Feszty, Gillies and Vezza, Ref. 5, have studied the use of a conventional trailing edge flap to alleviate dynamic stall. The investigations were made for a 16% chord flap on an NACA 0012 aerofoil oscillating in pitch. They found it was possible to greatly reduce the pitching moment break while maintaining the same lift as the uncontrolled aerofoil up to more than 22°. At maximum lift the controlled aerofoil generated 89% of the dynamic lift which was measured on the baseline uncontrolled section. This was achieved with the flap deflected for less than one quarter of the pitch cycle with a maximum deflection of 20°. The pitch cycle was sufficiently severe that full dynamic stall was reached both with and without the flap deflected. The effect of the flap was to displace the dynamic stall vortex and related trailing edge vortex to a higher position above the aerofoil.

Current helicopter envelopes are normally set conservatively away from full dynamic stall because of the high control loads which are produced by the pitching moment changes. The characteristics found in the movable flap study would allow a helicopter to penetrate much further into dynamic stall than is presently the case, with consequent benefits from using a considerable amount of dynamic lift.

4. Air-Jet Vortex Generators Air-jets are created by blowing air through holes in order to form three-dimensional vortex flow, quite similar to the flow produced by VGs and SBVGs. Their operation is indicated in Figure 2. The interaction with the flow downstream of the AJVG is similar to passive vortex generators at the same location. Effects when used near the leading edge include causing a laminar bubble to become turbulent and reattach and also to entrain additional air into this turbulent boundary layer and so delay turbulent separation.

Air-jets were originally proposed to control leading edge separation due to bubble bursting by Wallis, Ref. 6. The jets were placed on the lower surface of a NACA 64A006 aerofoil between the attachment line and the leading edge. Significant improvements in lifting performance were obtained, the lift coefficient at which serious separation was reached being increased from 0.65 to 0.86.

The most effective demonstrations of AJVGs to delay separation and increase maximum lift have been on two-dimensional aerofoils. Lewington, Peake, et al, Ref. 7, investigated the effect of AJVGs on a NACA 23012 aerofoil. A 25% increase in maximum normal lift coefficient was found when using rows of AJVGs at 12% and 62% chord and a blowing coefficient C_μ of 0.01. The enhanced lift was achieved by increasing effective stall incidence by 4°, and the stall-related drag increase and pitching moment break were delayed by similar margins. A single row at 12% gave a benefit almost as large as the double row, and a single row at 62% was less effective.

City University has also undertaken an additional investigation of pulsing the air supply instead of blowing continuously. This investigation of pulsed air supply follows research in the USA and UK, Ref. 8, which shows that the strength of the primary vortex is essentially a function of the time-averaged mass flow rate, but with additional benefit from the pulsing. In Ref. 8, tests are reported in a boundary layer tunnel with freestream airspeed of 32.6 m/s and pulsing the jet at 15 Hz. With the air supply open for only 25% of the pulse cycle and a peak velocity double the steady state blowing value (so that the pulsed test had half the mass flow rate of the steady test) the circulation in the primary vortex was greater with pulsing than the steady case. It is difficult to evaluate the desirability of pulsed blowing on rotor blades since the basic benefits have yet to be fully established for steady blowing. Indeed, one of the unknown factors is their performance on a helicopter rotor blade which, as it rotates around the azimuth, operates with different relative sweep angles to the oncoming flow. It is likely that it will be desirable to supply air to the AJVGs only for some part of the rotor azimuth which would be consistent with operation to alleviate a specific flow problem in one sector of the rotor disc.

5. Surface Blowing Circulation Control Blowing air tangentially to the aerofoil surface has been employed both at the leading and trailing edges of wings. The technique has been used by Wood and Roberts, Ref. 9, on the leading edge of a delta wing to increase the range of incidence over which there is stable vortex flow over the wing. This is not a circumstance directly relevant to rotorcraft, but it could be conjectured that there could be an application in modifying incipient dynamic stall behaviour. There would be difficulties in designing and manufacturing such a system, since the slot would need to be precisely engineered on a critical part of the aerofoil, where the boundary layer is thin. The design would have to be implemented in a manner which did not degrade performance when the system was not in use.

Blowing at the trailing edge to control circulation appears to be a much more promising concept. Englar, Ref. 10, Englar and Campbell, Ref. 11, Schaeffler et al, Ref. 12 and Jones et al, Ref. 13, have described the concept and fixed wing applications. The basic principle is to blow air rearward through a slot positioned by a semi-circular trailing edge, Figure 3. Under the Coanda effect the jet remains attached to the surface until separating at a considerable angle to the freestream flow, which modifies circulation in a similar way to a mechanical flap deflected at this position. The technique has been applied to rotorcraft, particularly in connection with high speed stopped rotor concepts. These vehicles have used thick elliptic aerofoils to give symmetry when the rotor is stopped and circulation control has been required to produce a reasonable lift/drag ratio from such inefficient sections. By contrast, the fixed wing research has concentrated on more conventional, if rather thick, aerofoils often employing circulation control to allow STOL performance without the need for complex mechanical high lift systems. The lift that can be generated by a circulation controlled system, particularly integrated with lift augmentation integrated with propulsion system, is such that Englar emphasises the benefits of his channel wing powered lift aircraft in meeting the objectives of a tilt-rotor vehicle. For augmenting the performance of a conventional helicopter the major concerns are the reduced efficiency of the modified basic aerofoil and the power required to provide the blowing air.

The aerofoils studied by Englar and Jones have a Coanda surface at the trailing edge in the form of a semi-circle with radius about 2% of the aerofoil chord. This makes a total thickness at the trailing edge of 4%, which is considerably in excess of a conventional rotor blade having a trailing edge thickness of about 0.6%. An investigation into the loss of effectiveness of the circulation control as the radius of the trailing edge is reduced below 2% would be required. With the 2% radius trailing edge, Jones used slots of height ranging from 0.1% to 0.2% of the aerofoil chord. On a typical helicopter blade this is less than 1mm and further reductions would be undesirable. The other possible route to avoid the thick trailing edge would be to investigate blowing at a position slightly forward of the trailing edge. Using high blowing speeds, a slot normal to the surface could achieve a similar if less efficient change in circulation, in the same way that a Gurney flap can increase lift even mounted slightly ahead of the trailing edge. The other question, of the power losses related to a blowing system, are difficult to estimate without undertaking a full vehicle design study. Assuming that it is not feasible to mount a pump on the outer part of the blade (in the vicinity of where the blowing is required), then any system will suffer the losses in ducting the air along the blade. In addition, losses in supply from the engines to the rotor system would be present.

6. Synthetic/Massless Jets These devices consist of a vibrating diaphragm at the base of a small cavity just under the aerofoil surface. A small hole through the surface allows the production of a stream of ring vortices travelling out from the surface, as shown in the schematic in Figure 4. Aerodynamically, this produces an interaction with the flow similar to that produced by AJVGs.

Hassan, Nagib and Wygnanski, Ref. 14, report a study of the effects of calculations and comparisons with experiments on a massless jet at 50% chord on a VR-7 helicopter aerofoil following earlier investigations, Ref. 15, on a NACA 0012 section. In static conditions the jet increased stall angle by about 4° with an associated increase in lift coefficient of about 0.3. This was accompanied by a pitching moment which, up to the 16° enhanced stall incidence, was more nearly constant than the pitching moment of the baseline aerofoil. However, at stall, the controlled aerofoil exhibited a much more severe pitching moment break.

Synthetic jets could be a lower power alternative to AJVGs and also have less effect than SBVGs when not in use. By comparison with AJVGs there is the ease of supplying power rather than air to the devices, but the local installation is significantly more complex than just a slot for the AJVG. In addition, since the air flow through the hole relies on oscillation of the air in the cavity, environmental blockage may be much harder to remove, making the devices susceptible to blocking by sand or water.

7. Surface Suction Holzhauser and Bray, Ref. 16, described the application of leading edge surface area suction to increase the maximum lift coefficient on a swept wing. This work, undertaken in the 1950s, included wind tunnel experiments and flight test on a North American F-86F. Maximum lift was increased by 70% with modest levels of suction. Given the structural and environmental constraints of the leading edge of a rotor blade, it is unlikely that any form of area suction would be a practical application to rotorcraft. Surface suction is also being studied as a means to reduce viscous drag by delaying laminar to turbulent boundary layer transition. Viscous drag reductions of the order of 20-30% have been assessed. Even with these potential gains, work is still underway to assess the engineering and cost of ownership issues. If the gains are still in the balance for fixed wing aircraft, it is considerably more dubious if there is potential on the rotary wing application.

8. Passive Porous/Slotted Surfaces Passive porous surfaces and spanwise slots have been found to be able to fix the position of shocks on wings, which may have some benefit for delaying buffet. However, an effect of the flow through the surface is to increase boundary layer thickness with a consequent increase in drag. It is doubtful that such devices could have any benefit for leading edge separation, smooth surface separation, or even shock induced separation if drag is significant, as it is on a rotorcraft.

There are also the alternative forms of slots represented by movable leading edge slats which include slots when extended. There is no doubt that the lift augmentation of slats could delay stall and increase lift on the retreating blade, but the practicality of such mechanisms on a rotor blade leading edge is extremely dubious. There are structural complications in mounting and actuating a slat on the critical leading edge part of the blade. In addition there are the mechanical complications of operating the device, which are more complex than actuating a trailing edge flap because of the form of linear and rotary motion required which does not lend itself to operation at the high speed required for once-per-rev extension and retraction.

9. Bumps or Localised Shaping Localised bumps provide a means to reduce shock strength. Ashill, Fulker and Shires, Ref. 17, described the use of a bump in the vicinity of a shock to reduce wave drag at off-design conditions and to slightly increase lift coefficient at which shock induced separation or buffet occur. There could be potential to reduce drag at the highest Mach numbers encountered on the advancing blade, but this is likely to be limited on existing rotor designs because planform and thickness are chosen to minimise the compressibility drag rise. A further

question with regard to rotor application is the unsteady nature of the flow, with the shock moving chordwise and appearing and disappearing during the blade rotation around azimuth. Localised shaping of the surface at the leading edge could increase high incidence performance, but this possibility is dismissed for rotorcraft given the environmental and structural constraints of installing such a system in the region occupied by the erosion shield.

10. Shark Skin or Riblets Shark skin or riblets is another feature described by Bechert, Ref. 18, as an application of lessons from nature. In this case the model is the skin of a shark which has a complex three-dimensional pattern which acts to reduce drag. This has been translated into two-dimensional riblets which have been produced as a film and shown to reduce aircraft drag. Experiments with three-dimensional patterns have failed to find a greater gain than those produced by the two-dimensional riblets. Skin friction reductions of up to 10% have been measured using riblets in nominally two-dimensional flow. The gains are reduced when the riblets are not aligned with the flow. Consequently it is unlikely that worthwhile benefits could result on the rotor blade, or perhaps any other part of a helicopter, given the unsteady varying flow directions on the vehicle.

Review of Candidate Rotorcraft Flow Control Devices

Various flow control devices have been reviewed, and their suitability for rotorcraft discussed. The highly unsteady nature of the rotor aerodynamic field makes it a hostile environment for flow control devices to operate within. However, four types of device have been identified as possible candidates, namely (i) SBVGs, (ii) AJVGs and (iii) movable flaps to delay stall, and (iv) surface blowing circulation control to augment lift. SBVGs are very effective for controlling separation, but will produce an amount of parasitic drag. They must also be placed close to the separation line, but their effectiveness at the range of flow angles encountered on a rotor blade is unknown. AJVGs produce aerodynamic effects similar to SBVGs, but are probably more suitable for rotorcraft, since they are flush mounted with the aerofoil surface and therefore do not suffer the drag penalty as with SBVGs. There is also the option of blowing air for selected conditions. Their most beneficial perceived effectiveness is in extending the stall incidence of the retreating blade, but a performance penalty due to the extra power required to pump air will be imposed. Movable flaps have been found to extend stall capability, but free operation on a rotor blade would not be acceptable. Therefore, some form of mechanical activation would be required. Trailing edge flaps could also be used to control vorticies formed during dynamic stall. Surface blowing at the trailing edge is an attractive option for changing the lift distribution on the rotor and their operation can be scheduled for maximum effect. However, like AJVGs, a penalty in terms of power required to pump air will be encountered. Design compromises of introducing a larger diameter cylindrical trailing edge, which would probably be required to maintain a suitable Coanda effect, may have additional detrimental aerodynamic effects.

Although the methods identified could provide the potential for step changes in rotor performance, it remains the case that there is a significant lack of data for flow control devices on rotor blade aerofoils, especially under the unsteady flow conditions which are a prime feature of rotor aerodynamics. Further research into these areas is required.

Computational AJVG Modelling

A number of researchers have studied the capability of CFD based numerical methods to accurately simulate air-jets and their influence on the generated vortex behaviour. Ref. 19 discusses numerical simulations of an AJVG issuing into a boundary layer flow over a flat plate, using the k-ε turbulence model. The analyses are based upon discussions of the skin friction behaviour downstream of the AJVG, where an increase in this parameter is considered beneficial due to a thinning of the boundary layer and hence a delay in the onset of separation. An optimum air-jet pitch of ϕ=30° and skew of ψ=60° were identified to provide maximum skin friction enhancement. It was also considered that the geometry of the AJVG had little effect on the resulting vortices, providing the mass flux was kept constant. A similar conclusion was also reached by Zhang, Ref. 20, who studied the effects of air-jets issuing through round jet nozzles into a flat plate boundary layer flow. The influence of the jet inflow boundary condition was studied by comparing a flat 'top-hat' velocity profile with a fully developed velocity profile (as would be the case due to the influence of the AJVG feeding tube). A conclusion was drawn that, for the case studied, the profile had no significant impact on the predicted vortex development, providing the mass flux was kept constant. This study also concluded that a Reynolds Stress Transport model should be used to predict accurately the basic features of the mixing flowfield. Other important research, as considered in Ref. 8 and Ref. 21, conducted numerical research into AJVGs issuing into flat plate boundary layer flows. The latter reference makes some headway into predicting the flow on a flat plate under a strong streamwise favourable/adverse pressure gradient, as would be encountered by an aerofoil.
The research discussed in this paper is dedicated to the prediction of AJVG behaviour over an aerofoil at a high angle of attack. The main aim of the present research is to determine which CFD model predicts the basic beneficial trends, as observed in experiment, of aerofoils incorporating AJVG flow control technology.

RAE9645 Test Case

Experimental research into rotorcraft AJVG operation within the UK is being led by City and Glasgow Universities. Research has concentrated on studying the effects of blowing air through co-rotating AJVGs under (i) quasi-steady (static aerofoil) conditions, investigating the effects of continuous and pulsed blowing, and (ii) unsteady (oscillating aerofoil) conditions on NACA 23012C and RAE9645 aerofoil sections. Results have shown significant benefits of AJVG operation in delaying stall (including dynamic stall) with relatively low amounts of blowing, and expanding the aerofoil performance envelope. Full details of the experimental results can be found in Ref. 7 and Ref. 22.

The present computational study is based upon the Glasgow experiments, Ref. 22, which employed co-rotating AJVGs on an RAE9645 aerofoil section. This particular aerofoil forms the mid to outer part of the complete BERP III blade, Ref. 23, and generates most of the rotor lift in hover and also in the fore and aft sectors during high speed flight and key retreating blade stall sector. The model aerofoil, of chord c=0.5m, consisted of two rows of AJVGs placed at 12% and 62% chord. The AJVGs were pitched at ϕ=30° relative to the suction surface tangent and skewed at ψ=60° relative to the oncoming flow. Although the experiments investigated various blowing rates, AJVG combinations and quasi-steady/unsteady environments, this computational study concentrates on the static aerofoil results at a blowing coefficient C_μ=0.011 from the 12% chord AJVG row only. These tests were carried out at Re_c=1.5 million with M_∞=0.13. Figure 5 shows the observed experimental aerodynamic benefit at α=18°. Unsurprisingly for the unblown case, most of the flow over the suction surface has separated, and the aerofoil is operating in the post-stall region. With the AJVG active, the suction surface C_p monotonically decreases to zero at the trailing edge, and the flow remains attached. For this case, the suction surface pressure redistribution results in a normal lift coefficient increase from 1.26 (stalled) to 1.65 (pre-stall).

CFD Approach – Initial Considerations

All CFD computations were carried out using the commercially available Fluent v.6 solver, Ref. 24. This cell-centred finite volume code was run in a steady-state compressible mode to solve the Reynolds Averaged Navier-Stokes equations. In order to succeed in accurately predicting the complex flow interaction between the air-jet and the oncoming aerofoil flow, and hence predict the performance benefits as seen from experiment, it was first vital to validate the code against the unblown RAE9645 aerofoil data. To this end, 2d grid dependency studies and turbulence model studies at a range of α were first undertaken, with the best performing turbulence models then being carried through to incorporate AJVGs in full 3d CFD calculations.

CFD Approach – AJVGs - DMA vs STA

Two separate CFD approaches to modelling the effects of AJVGs are identified. The first, namely the Direct Modelling Approach, DMA, requires the direct modelling of both the AJVG geometry on the blade suction surface and the physical interaction of the jet with the oncoming boundary layer flow. This approach has the advantage of directly accounting for any AJVG geometry related effects that may be present, however, the grid sizes are inherently large. The second method, termed the Source Term Approach, STA, implements a source term model which introduces a side force to the flow that would be created by a vaned vortex generator. This method has been successful in recreating the flow effects generated by an array of VG vanes, as described in Ref. 25, where a grid reduction of approximately 70% was achieved when compared to a solution using the DMA approach. For AJVGs, a vane equivalence model would need to be established, so that the vorticity field as produced by the AJVG would be recreated by an equivalent vane side force. This method would better lend itself to any unsteady CFD computations due to the much reduced grid sizes. However, unless detailed high quality experimental data were available, the STA approach could only be tuned and validated by comparing the results to a DMA solution. Due to time limitations, the computations discussed in this report only use a DMA CFD approach.

CFD Approach – Grid Generation

All 2d aerofoil meshes were generated as structured C-grids, as shown in Figures 6(a) and 6(b). Farfield boundary conditions were imposed on the outer domain edges and were placed 20-25 blade chords from the aerofoil. 2d grid dependency checks were performed, and the first cell heights around the aerofoil were placed such that they conformed with the requirements of the wall functions that were employed for all of the computational investigations.

Figure 6(c) shows the approach taken for the 3d grids that were required to model AJVGs. In order to maintain the structured nature of the grid and hence consistency with the 2d grids, the 3d grid was body-fitted around the AJVG slot, which can be identified as the blue rectangular area on the suction surface. The original 3d grid maintained a radial grid expansion equal to the 2d grids. The streamwise grid spacing was also kept consistent with the 2d grids, except to account for the extra mesh required around the AJVG location. The spanwise grid spacing consisted of 70 cells which were required to maintain a suitable grid expansion from the AJVG to the blade spanwise extents. The AJVG spanwise spacing was set to s=0.045m. The spanwise centre-point of the AJVG slot was positioned at z/s=0.60. The AJVG slot was modelled with a grid containing 512 quadrilateral cells. For the 3d cases, the spatial node locations of corresponding grid points on both '2d' grids at the spanwise extents, i.e. Figure 6(a) grids, were kept consistent, so that a translational periodic boundary could be applied, as required to model the co-rotational effects of the AJVGs.

2d Aerofoil CFD Validation

CFD code validation began by identifying the mesh density required to give grid independent solutions. This was determined with the standard k-ε turbulence model. Further investigations were then undertaken to assess the performance of various turbulence models, as listed below.

1. Spalart-Allmaras (SA)
2. Standard k-ε
3. Realizable k-ε
4. RNG (Renormalisation Group) k-ε
5. Standard k-ω

6. Shear-Stress Transport k-ω
7. Reynolds Stress Model (RSM)

Effort was initially concentrated on obtaining results for the RAE9645 at the freestream conditions of Re_c=1.5 million and M_∞=0.13, at an aerofoil pitch of α=18°. Figure 7(a) and 7(b) show the predicted variation of C_p vs. x/c and y/c, compared to experiment. All models predict a negative C_p at the trailing edge and a large separation, in line with experiment. However, it can be seen that the SA turbulence model generally predicts the overall C_p trend the most accurately. Both k-ω models also predict the trend to a fair degree, but spurious flow features downstream of the trailing edge, which remained with further grid refinement, cast doubt on their ability to fully resolve the flowfield away from the aerofoil surface for this particular flight condition. The standard k-ε model performed less well than the SA model in terms of the abrupt flattening of the C_p curve within the 0.2<x/c<0.3 range, but the peak values of C_p are predicted best by this model. The two variations of the standard k-ε turbulence model, along with the RSM model gave the worst predictions, greatly over-predicting the leading edge suction and failing to accurately capture the flow separation. It was therefore decided to concentrate effort with the standard k-ε and SA turbulence models.
To check the chosen turbulence model performance at other aerofoil incidences, the RAE9645 was computed at the same freestream flight condition at α=10° and 15° with the standard k-ε model and the SA model. The results are shown in Figures 8(a) and 8(b). Both models predict the aerofoil pressure distribution well, with the standard k-ε turbulence model slightly out-performing the SA turbulence model in terms of overall experimental match and maximum suction surface C_p.
Predictions of 2d aerofoil normal force coefficient, C_N, are also compared with experiment for both turbulence models in Figure 9. This figure shows that both models predict very similar lift variation in the linear part of the curve, which matches well with experiment. However, the SA model appears to fall down at negative aerofoil incidence. Nearer the stall region, which occurs at approximately α=15°, the standard k-ε turbulence model predicts better overall levels of C_N, whereas the SA turbulence model tends to better predict the rapid drop in lift within the stall region.
Both the standard k-ε and SA turbulence models generally give good overall aerodynamic and performance predictions of the RAE9645 at this particular Re_c and M_∞. These models were chosen as the final candidates to progress to 3d CFD computations of the RAE9645 incorporating co-rotating AJVGs at the 12% chord position. These results are described in the next section.

3d AJVG CFD

Initial 3d CFD computations were performed on an unblown aerofoil, in order to check consistency of results between a 2d model and a 3d model incorporating periodic boundaries. To achieve this, the AJVG inlet, coloured blue in Figure 8(c), was simply set to a viscous wall boundary condition. The results with the standard k-ε turbulence model confirmed both approaches gave compatible results.
Table 2 lists the 3d CFD cases that were employed for the computational studies. The 'Original' grid, consisting of 2,210,880 hexahedral cells was derived from the 2d grids, but incorporates a greater number of streamwise grid points to take account of the presence of the AJVG geometry. The 'Fine' grid increased the number of cells radiating out from the suction and pressure surfaces, thereby refining the grid within the boundary layer (the wall adjacent cells were not modified, so that y^+ values were still within acceptable limits as required by the wall functions). The 'Fine' grid consisted of 2,632,000 hexahedral cells. Due to initially disappointing results with the standard k-ε turbulence model, two modifications were made to Case 2 in order to assess mass flux and jet velocity ratio impact on the results. First of all, the AJVG area was doubled, thereby doubling the mass flow and C_μ values, as detailed in Table 2 for Case 5. This changed the AJVG aspect ratio from its original value of approximately 4 (looking directly down onto the AJVG slot) to about 2. Secondly, the jet velocity ratio was increased to a relatively high value of 5, as detailed for Case 6. All 3d CFD computations performed with active AJVGs set an appropriately angled 'top-hat' velocity boundary condition on the aerofoil suction surface to represent the air-jet issuing into the oncoming boundary layer flow at a pitch of φ=30° and a skew of ψ=60°.

3d AJVG CFD - Skin Friction Enhancement

As described earlier, enhanced skin friction levels on the suction surface are desirable, since they help to keep the boundary layer attached. Figure 10 compares the influence that the air-jet development and subsequent propagation has on the suction surface skin friction. A notable feature across all active AJVG predictions (Cases 2-6) is that two distinct footprints, or 'tails' of high skin friction emanate from the AJVG, with the strongest tail developing at the furthest downstream edge of the AJVG rectangular slot (on the right-hand side of the slot as shown in the Figure). All the standard k-ε turbulence model results showed similar jet dissipation rates, even with increased mass flow, as for Case 5, and with a high jet velocity, Case 6. The most striking difference comes with a change of turbulence model to SA, Case 4, where the skin friction footprint is wider and persists for a greater streamwise distance. These differences can be observed more easily by displaying plots of skin friction at different streamwise positions. The spanwise variation of C_f at 16%, 20% and 30% chord for each of the 6 cases are shown in Figures 11(a), 11(b) and 11(c) respectively. The plots at 16% chord show the double peak for each active AJVG case, representing the two 'tails', as observed in the contour plots of Figure 10. The Case 1 unblown predictions show a small difference in baseline skin friction coefficient between the standard k-ε and SA turbulence models. Cases 2 and 3 show no major differences, suggesting that grid refinement has not affected the initial vortex development. The SA turbulence model of Case 4 generally predicts the same C_f variation as its standard k-ε turbulence model counterparts, but with a slightly wider range of C_f and the two 'tails' slightly closer together. Case 5 shows its two peaks at different locations, due to the change in AJVG aspect ratio, whilst the major effect of a VR increase is to greatly increase the C_f value. Plots at 20% and 30% chord show a rapid decrease in skin friction for the standard k-ε cases, but the SA case, Case 4, encounters an increase to 20% chord and then a more gradual decrease. The SA model also shows the two C_f peaks to have merged by 20% chord, whereas this occurs for the standard k-ε cases by 30% chord. The persistence of the vortex to propagate downstream for the SA turbulence model compared with the standard k-ε turbulence model is illustrated in Figure 12, which compares in-plane velocity vectors and contours of streamwise vorticity for Cases 3-6. Each standard k-ε case, including the increased blowing of Cases 5 and 6, show very rapid vortex dissipation rates. The increased blowing cases tend to promote a greater rate of vortex 'lift-off' from the suction surface. The ability of the SA turbulence model to retain vortex core strength would suggest that it may be suitable in recreating the beneficial aerodynamic effects of AJVGs to delaying flow separation and expanding the blade operating envelope. Indeed, the C_p plot in Figure 13 which compares the 2d unblown aerofoil pressure distributions with those of the corresponding 3d distributions (Cases 3 and 4), show that only the SA model redistributes and raises the peak C_p around the suction surface leading edge region and hence modifies the resulting lift force. Although not an exact match with experiment, this current solution (Case 4) shows the correct experimental trend when comparing the clean aerofoil characteristics with an aerofoil incorporating AJVGs. The predicted C_N value rises from 1.22 to 1.65, which corresponds well to experiment. However, this solution still shows a degree of separated flow, with flow recirculation occurring on the suction surface at x/c=0.72. Nevertheless, the mechanisms by which the vortex generation, interaction with the boundary layer and subsequent propagation must, in part, be able to be predicted by using the Spalart-Allmaras turbulence model. This seems to be the case, at least, for this particular geometry, grid and operating condition.

Rotor Performance Modelling with AJVGs

An early evaluation of the effect of including AJVG control technology as a helicopter rotor performance enhancement was undertaken using the Coupled Rotor-Fuselage Model (CRFM) code, Ref. 26. Modifications to aerofoil performance data based on the Glasgow University RAE9645 experimental results were incorporated into the aeroelastic analysis tool for isolated rotors in order to explore possible extensions to the flight envelope. The code allows the specification of generic incremental changes of lift and pitching moment over specified ranges of the azimuth to simulate the addition of performance enhancing devices to the rotor. An iterative approach was used to find the maximum forward speed of the rotor with and without the benefit of the simulated AJVGs in delaying stall on the retreating blade.

Preliminary results suggest that an increase in maximum forward speed of around 20kts may be possible using AJVG technology on a medium class helicopter. Studies into the possibility of increasing the all-up mass are also being undertaken, although the gains shown so far are less significant than the potential increase in forward speed.

With an increased maturity of the CFD predictions, it is anticipated that further potential benefits in performance can be assessed in a similar manner, using the CFD results directly in place of the experimental results. System level efficiency studies will also be required to assess the power required to generate sufficient levels of bleed air.

Conclusions

A range of flow control devices are reviewed for their suitability to suppress or eliminate various aerodynamic flow phenomena. Specifically, those devices which may lend themselves to control the flow on helicopter rotor blades are identified. Four types of device have been identified as possible candidates, namely (i) SBVGs, (ii) AJVGs and (iii) movable flaps to delay stall, and (iv) surface blowing circulation control to augment lift. Although the methods identified could provide the potential for step changes in rotor performance, it remains the case that there is a significant lack of data for flow control devices on rotor blades, especially under the unsteady flow conditions which are a prime feature of rotor aerodynamics. Further research into these areas is required.

Computational Fluid Dynamics analyses of a static RAE9645 section incorporating a row of co-rotating AJVGs at 12% chord at Re_c=1.5million and M_∞=0.13 were undertaken and compared with experimental results. A range of turbulence models were tested, and it was concluded that only the Spalart-Allmaras model was capable of predicting both the unblown and blown aerofoil characteristics for this flight condition. The standard k-ε model was seen to dissipate the generated vortex too quickly for the vortex to have a positive impact in delaying the onset of stall. This was also the case for blowing rates and jet velocity ratios higher than the experimental values.

Rotor performance codes were also used to predict the operational advantages of employing AJVG flow control technology in helicopter rotor blades. Initial predictions indicate that an increase in maximum forward speed of around 20kts may be possible. Studies into the possibility of increasing the all-up mass currently indicate less benefit.

Further Work

Further CFD analyses should be undertaken on the static RAE9645 section geometry incorporating air-jets and the results compared with experiment across a range of incidence. Once the model has been suitably validated, work should be concentrated in two areas. First of all, a Source Term Approach model should be developed, so that accurate CFD predictions can be made on much coarser grids. This will allow progress to be made using unsteady CFD methods to predict air-jet behaviour on oscillating aerofoils. Secondly, CFD investigations of air-jets at higher Reynolds number flows, more representative of rotor blades, should be investigated.

Acknowledgements

This research has been undertaken by QinetiQ with Ministry of Defence funding through the "Exploitation of Flow Control" Corporate Research Programme.
The authors would also like to thank Mr. M.J. Williams and Mr. A.J. Timewell of QinetiQ for their helpful contributions.

References

1. Ashill P R, Fulker J L, Hackett K C, *"Research at DERA on sub boundary layer vortex generators"*, AIAA 2001-0887.
2. Humphreys C, Smith L, *"Steady state results from tests in the ARA two-dimensional wind tunnel on the RAE9645 aerofoil section with a trailing edge device"*, ARA model test note G71/2, Sept 1993.
3. Kaynes I W, *"Smart Rotor Research in the UK"*, 58th Annual Forum of the American Helicopter Society, Montreal, Canada, 11-13th June 2002.
4. Bechert D W, Bruse M, Hage W, Meyer R, "*Biological surfaces and their technological application - laboratory and flight experiments on drag reduction and separation control"*, AIAA 97-1960, July 1999.
5. Feszty D, Gillies E, Vezza M, "*Alleviation of rotor blade dynamic stall via trailing edge flap flow control"*, AIAA 2003-050, Reno, January 2003.
6. Wallis R A, "*Experiments with air jets to control the nose stall on a 3ft chord NACA 64A006 aerofoil*", Aero. Notes. Aero. Res. Lab., Melbourne 139, 1954.
7. Lewington N P, Peake D J, Henry, F S, Kokkalis A, Perry J, *"The application of air-jet vortex generators to control the flow on helicopter rotor blades"*, 26th European Rotorcraft Forum, The Hague, Netherlands, 26-29th September 2000.
8. Tilmann C P, Langan K J, Betterton J G, Wilson M J, *"Characterization of pulsed vortex generator jets for active flow control"*, presented at RTO AVT symposium on "Active Control Technology for Enhanced Performance Operational Capabilities of Military Aircraft, Land Vehicles and Sea Vehicles, Braunschweig, Germany, 8-11th May 2000.
9. Wood N J, Roberts L, "*Control of vortical lift on delta wings by tangential leading edge blowing"*, Journal of Aircraft, Vol.27, 1990.
10. Englar R J, "*Circulation control pneumatic aerodynamics: blown force and moment augmentation and modification; past, present and future"*, AIAA paper 2000-2541.
11. Englar R J, Campbell B A, "*Pneumatic channel wing powered-lift advanced super-STOL aircraft"*, AIAA 2002-3275, AIAA Flow control conference, St Louis, June 2002.
12. Schaeffler N W, Hepner T E, Gregory S, Kegerise M A, "*Overview of active flow control actuator development at NASA Langley Research Center"*, AIAA 2002-3159.
13. Jones G S, Viken S A, Washburn A E, Jenkins L N, Cagle C M, "*An active flow circulation controlled flap concept for general aviation aircraft applications"*, AIAA 2002-3157, AIAA Flow control conference, St Louis, June 2002.
14. Hassan A A, Nagib H, Wygnanski I. "*Oscillatory jets - benefits and numerical modeling issues"*, American Helicopter Society 58th Forum, Montreal, June 2002.
15. Hassan A A, JanakiRam R D, "*Effects of zero-mass synthetic jets on the aerodynamics of the NACA0012 airfoil"*, AIAA paper 97-2326, 1997.
16. Holzhauser C A, Bray R S, "*Wind tunnel and flight investigations of the use of leading edge area suction for the purpose of increasing maximum lift coefficient of a 35^o swept wing airplane"*, NACA Rep 1276, 1956.
17. Ashill P R, Fulker J L, Shires A, "*A novel technique for controlling shock strength of laminar-flow aerofoil sections"*, Unpublished DRA Report.
18. Bechert D W, Bruse M, Hage W, Meyer R, "*Biological surfaces and their technological application - laboratory and flight experiments on drag reduction and separation control"*, AIAA 97-1960, July 1999.
19. Henry F S, *"Numerical model of boundary-layer control using air-jet generated vorticies"*, AIAA Journal, Vol 32, No 12, December 1994, pp. 2415-2424.
20. Zhang X, Zhang H_L, Collins M W, *"Some aspects of streamwise vortex production using air jets"*, presented at the 34th AIAA Aerospace Science Meeting, January 15-18th, 1996, Reno, USA.
21. Lewington N P, Henry F S, Peake D J, Singh C, *"Numerical and experimental investigations of air-jet vortex generators in streamwise pressure gradients"*, The Aeronautical Journal, July 2001, pp. 401-407.
22. Singh C, Peake D J, Kokkalis A, Coton F, Galbraith R, *"Control of flow on helicopter rotor blades under quasi-steady and unsteady conditions using smart air-jet vortex generators"*, 29th European Rotorcraft Forum, Friedrichshafen, Germany, 16-18th September 2003.
23. Perry F J, "*Aerodynamics of the helicopter world speed record*", American Helicopter Society, 43rd Annual National Forum, May 1987.
24. Fluent 6 User Guide, Fluent Inc., December 2001.
25. Waithe K A, *"Source term model for an array of vortex generator vanes"*, NASA/CR-2003-212157, March 2003.
26. Young C, "*The implementation of the Coupled Rotor-Fuselage Model at DERA*", Unpublished DERA Report.

Table 1: Matrix of flow control methods, types of flow control and applicability to rotorcraft

Flow Control Device	Flows to be Controlled: Leading Edge Separation (control of leading edge thrust/lift-dependant drag	Smooth Surface separation	Shock-induced separation	Viscous Drag	Wave Drag	Vortex Bursting	Operational/Power: Power Requirement	Operational Performance	Suitability for Rotorcraft
VG's	Suitable	Suitable	Suitable	Uncertain	Unsuitable	Suitable	Suitable	Unsuitable	Unsuitable
SBVG's	Suitable	Suitable	Suitable	Uncertain	Unsuitable	Suitable	Suitable	Uncertain	Uncertain
Movable Flaps	Unsuitable	Suitable	Suitable	Uncertain	Unsuitable	Unsuitable	Suitable	Suitable	Suitable
AJVG's	Suitable	Suitable	Suitable	Uncertain	Unsuitable	Suitable	Uncertain	Suitable	Suitable
Surface Blowing CC	Suitable	Suitable	Suitable	Unsuitable	Suitable	Suitable	Uncertain	Suitable	Suitable
Synthetic or Massless jets	Uncertain	Suitable	Uncertain	Uncertain	Unsuitable	Uncertain	Suitable	Uncertain	Uncertain
Surface Suction	Suitable	Suitable	Suitable	Suitable	Unsuitable	Suitable	Uncertain	Unsuitable	Unsuitable
Passive porous or slotted surfaces	Uncertain	Uncertain	Suitable	Unsuitable	Suitable	Unsuitable	Suitable	Unsuitable	Unsuitable
Bumps or localised shaping	Uncertain	Unsuitable	Suitable	Unsuitable	Suitable	Unsuitable	Suitable	Unsuitable	Unsuitable
Shark skin or riblets	Unsuitable	Uncertain	Unsuitable	Suitable	Unsuitable	Unsuitable	Suitable	Unsuitable	Unsuitable

Prospects	Suitable	Uncertain	Unsuitable

Table 2 : 3d CFD computational models

CASE	Grid	Turbulence Model	C_μ	Velocity Ratio VR	Notes
1	Original	Std k-epsilon	0.0000	0.00	3d Baseline
2	Original	Std k-epsilon	0.0109	2.67	-
3	Fine	Std k-epsilon	0.0109	2.67	Boundary layer mesh refinement
4	Fine	Spalart-Allmaras	0.0109	2.67	-
5	Original	Std k-epsilon	0.0217	2.61	Air-jet slot area doubled
6	Original	Std k-epsilon	0.0376	5.00	Jet velocity ratio increased

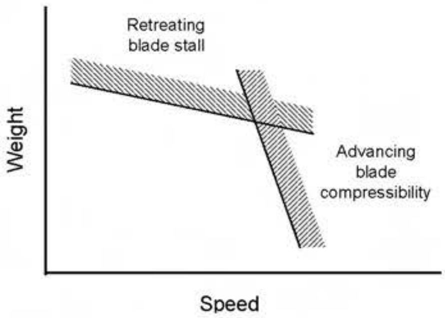

Figure 1 : Typical weight-speed envelope

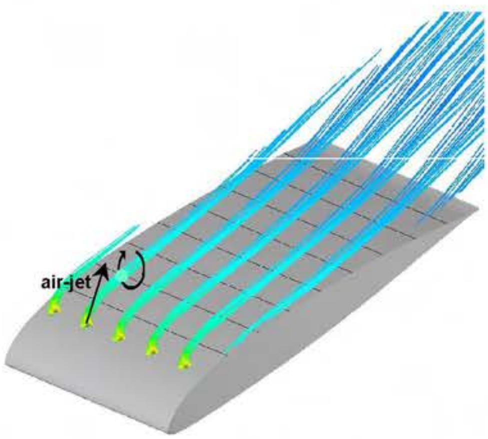

Figure 2 : Co-rotating air-jet vortex generators

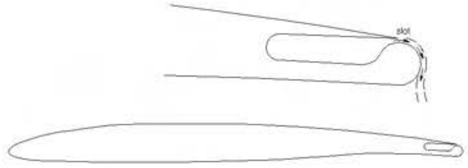

Figure 3 : Aerofoil trailing edge circulation control schematic

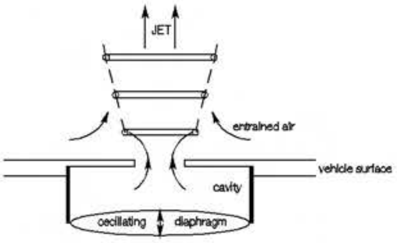

Figure 4 : Synthetic jet schematic

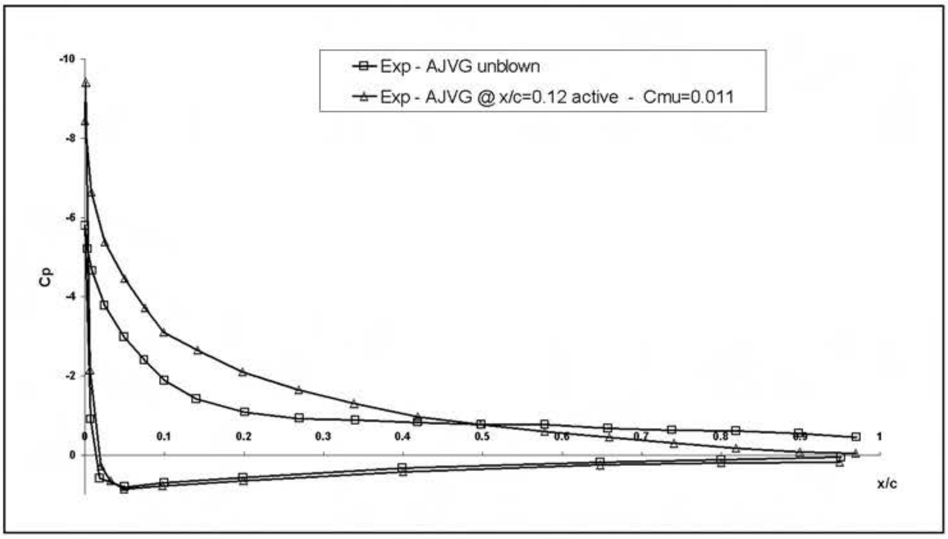

Figure 5 : Glasgow University RAE9645 experimental chordwise surface pressure distribution for AJVG row at x/c=0.12, α=18°, Re_c=1.5x10^6 and M_∞=0.13; unblown vs. active AJVG, from Ref. 22

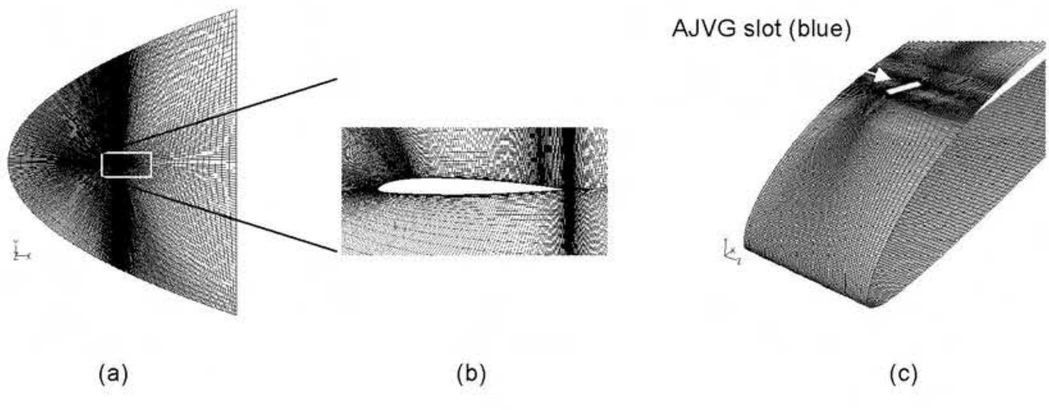

Figure 6 : RAE9645 CFD grid details

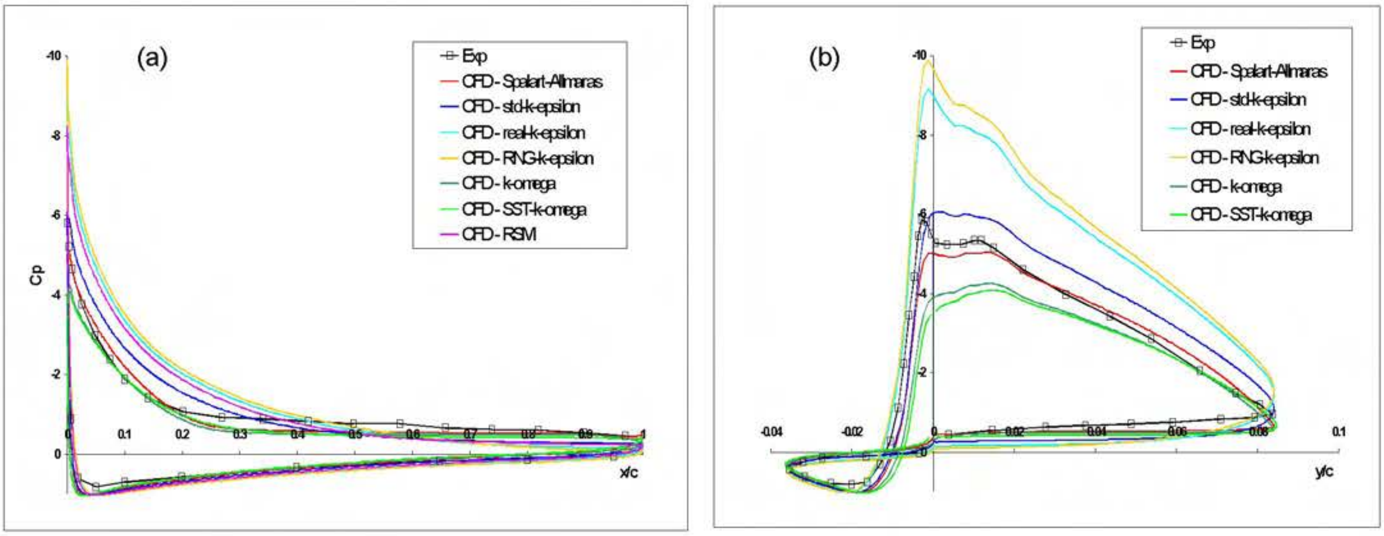

Figure 7 : Effect of turbulence model on the unblown RAE9645 (a) chordwise surface pressure distribution and (b) leading edge suction; $\alpha=18°$, $Re_c=1.5x10^6$ and $M_\infty=0.13$

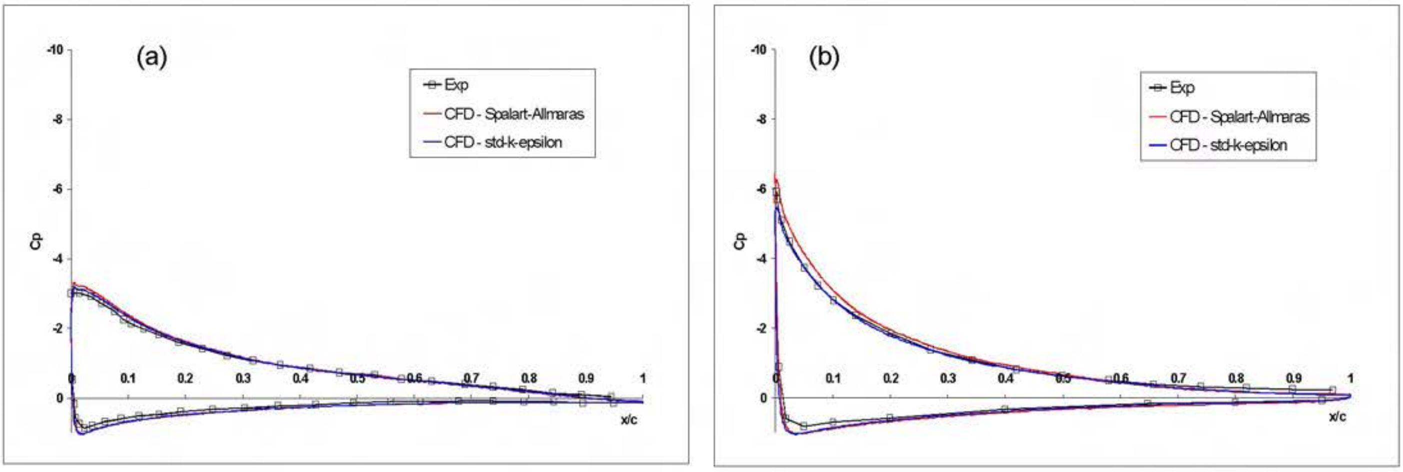

Figure 8 : Unblown RAE9645 chordwise surface pressure distributions at (a) $\alpha=10°$ and (b) $\alpha=15°$; standard k-ε and Spalart-Allmaras turbulence models; $Re_c=1.5x10^6$ and $M_\infty=0.13$

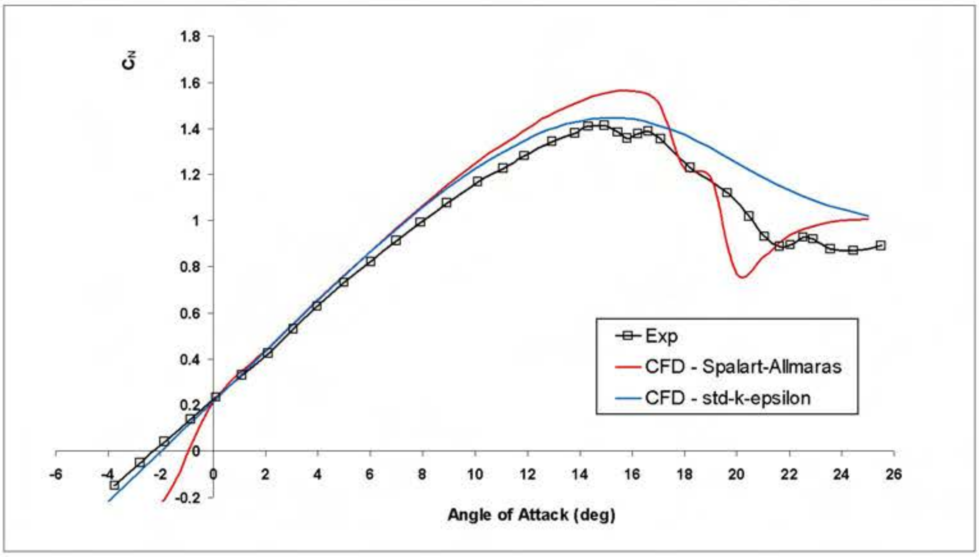

Figure 9 : Unblown RAE9645 normal force coefficient - standard k-ε and Spalart-Allmaras turbulence models; $Re_c=1.5x10^6$ and $M_\infty=0.13$

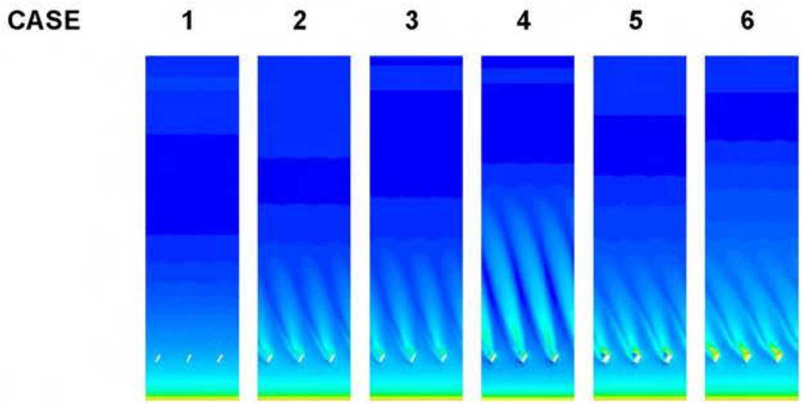

Figure 10 : Predicted suction surface skin friction coefficient contours – 3d CFD Cases 1-6 (Table 2)

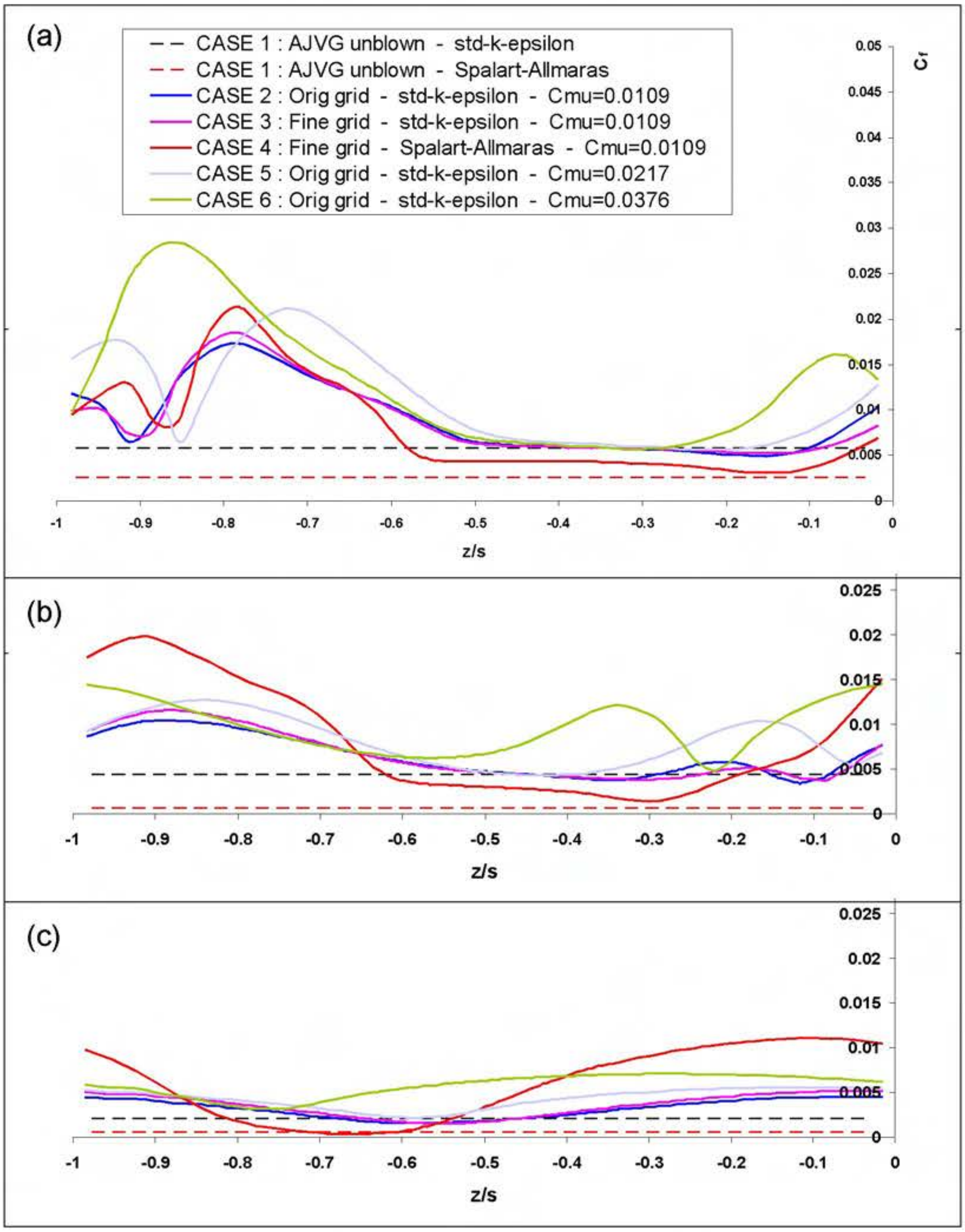

Figure 11 : 3d CFD predicted skin friction coefficient plots at (a) x/c=0.16, (b) x/c=0.20 and (c) x/c=0.30

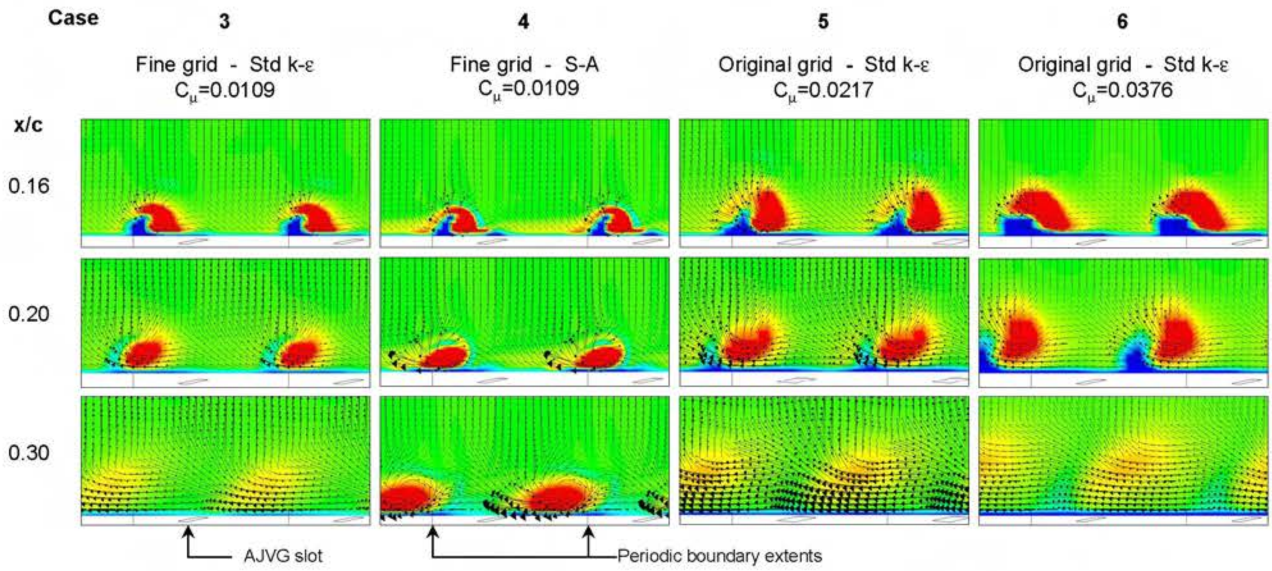

Figure 12 : 3d CFD predicted streamwise vorticity contours and transverse velocity vectors – Cases 3-6 (Table 2)

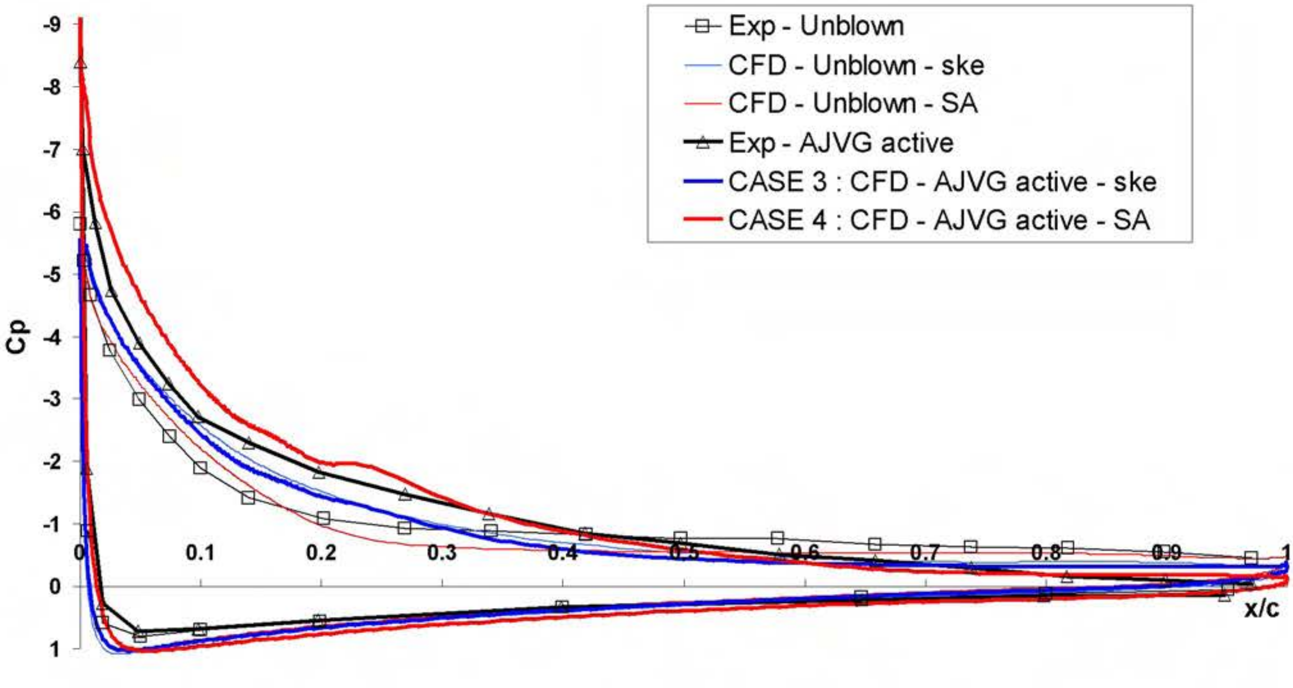

Figure 13 : 3d CFD predicted RAE9645 chordwise surface pressure distributions – effect of blowing with the standard k-ε and Spalart-Allmaras turbulence models; α=18°, Re_c=1.5x10^6 and M_∞=0.13